International Journal of Thermal Sciences 49 (2010) 1165–1174

Contents lists available at ScienceDirect

International Journal of Thermal Sciences

journal homepage: www.elsevier.com/locate/ijts

Pressure-driven electrokinetic slip-flow in planar microchannels

J. Jamaati [a], H. Niazmand [a], M. Renksizbulut [b,*]

[a] Ferdowsi University of Mashhad, Mechanical Engineering Department, Mashhad, Iran
[b] University of Waterloo, Mechanical & Mechatronics Engineering Department, Waterloo, Ontario, Canada N2L 3G1

ARTICLE INFO

Article history:
Received 26 June 2009
Received in revised form
26 November 2009
Accepted 10 January 2010
Available online 18 February 2010

Keywords:
Electrokinetic flow
Poisson–Boltzmann equation
Slip-flow
Microchannel

ABSTRACT

This paper presents an analytical solution for pressure-driven electrokinetic flows in planar microchannels with velocity slip at the walls. The Navier–Stokes equations for an incompressible viscous fluid have been solved along with the Poisson–Boltzmann equation for the electric double layer. Analytical expressions for the velocity profile, average electrical conductivity, and induced voltage are presented without invoking the Debye–Hückel approximation. It is known that an increase in the zeta-potential leads to an increase in the flow-induced voltage; however, it is demonstrated that the induced voltage reaches a maximum value at a certain zeta-potential depending on the slip coefficient and the Debye–Hückel parameter, while decreasing rapidly at higher zeta-potentials. The present parametric study indicates that liquid slip at the walls can increase the maximum induced voltage very significantly.

1. Introduction

Microfluidic systems have become increasingly attractive in a variety of engineering fields such as micro power generation and biochemical processing due to recent advances in microfabrication technologies. Precise control of such systems often requires a complete understanding of the interaction between fluid dynamics and the electrical properties of the microchannel; usually referred to as electrokinetics. In every electrokinetic application, finding the accurate distribution of the prevailing electric potential is of fundamental importance, which is governed by the non-linear Poisson–Boltzmann (P–B) equation in many cases. The linear form, following the Debye–Hückel (D–H) approximation, is only valid when the electrical potential is small compared to the thermal energy of the ions.

Different methods have been developed for the solution of the P–B equation. Exact solution of the P–B equation between two dissimilar planar charged surfaces is presented by Behrens and Borkovec [1] in terms of Jacobian elliptic functions. A similar approach has been employed by other researchers [2–5] for the evaluation of streaming current and electrokinetic energy conversion. Although this semi-numerical scheme is capable of solving the non-linear P–B equation, the resulting potential filed cannot be expressed in a closed form solution, and therefore, it is not suitable for fully analytical investigations of the flow field. There have been several attempts to extend the analytical solution of the P–B equation for a single flat plate [6] to a planar microchannel with overlapping electric double layers (EDLs) [7–10]. However, such a treatment requires a detailed examination of the key parameters, which has not received proper attention in the literature. Dutta and Beskok [10] derived an analytical expression for the velocity distribution in mixed electro-osmotic/pressure-driven channel flows based on Hunter's solution [6] for a flat plate. Min et al. [9] studied the electro-pumping effects in electro-osmotic flows and determined the flow rates both analytically and experimentally. In their analytical treatment, Hunter's solution is employed and a criterion for the applicable range of the solution is developed. Oscillating flows in two-dimensional microchannels were analytically studied by Wang and Wu [7]. Their analysis is also based on Hunter's non-linear P–B solution and velocity profiles are presented for thin EDLs; however, the conditions for the validity of the solution are not clearly discussed.

For highly overlapped EDLs, the use of the Boltzmann equation may lead to inaccurate potential distributions as indicated by Qu and Li [11]. Yet, there are various studies involving strongly overlapped EDLs ($K < 10$) in which the P–B equation has been used [1–3]. For these cases, a new set of governing equations and boundary conditions such as the charge regulation model have been proposed [11–14], where chemical equilibrium conditions in conjunction with overall charge and mass conservation of the ionic species are considered. However, the analytical treatment of these models is limited by the Debye–Hückel approximation [11,12].

* Corresponding author. Tel.: +1 519 888 4567; fax: +1 519 885 5862.
E-mail address: metin@uwaterloo.ca (M. Renksizbulut).

1290-0729/$ – see front matter © 2010 Elsevier Masson SAS. All rights reserved.
doi:10.1016/j.ijthermalsci.2010.01.008

Nomenclature

B	ratio of ionic pressure to dynamic pressure, $B = k_b T_{ref} n_0 / \rho U_{ref}^2$
D	species diffusion coefficient [m^2/s]
e	elementary charge, $e = 1.602 \times 10^{-19}$ [C]
E_x	induced voltage, $E_x = E_x^*/(\psi_{ref}/H)$
H	microchannel height [m]
I	electric current density, $I = I^*/I_{ref}$
I_{ref}	reference current density, $I_{ref} = \rho_{e,ref} U_{ref}$ [C/m^2 s]
J_s, J_c	local streaming and conduction current densities, $J = J^* H / I_{ref}$
K	dimensionless Debye–Hückel parameter, $K = \kappa H$
k_b	Boltzmann constant, $k_b = 1.381 \times 10^{-23}$ [J/K]
L	microchannel length, $L = L^*/H$
n_o	bulk ionic concentration [ions/m^3]
P	pressure, $P = P^*/\rho U_{ref}^2$
q_s	surface charge density, $q_s = q_s^*/H\rho_{e,ref}$
Re	Reynolds number, $Re = \rho U_{ref} H/\mu$
Sc	Schmidt number, $Sc = \mu/\rho D$
T	absolute temperature, $T = T^*/T_{ref}$
T_{ref}	reference temperature [298 K]
u	axial velocity, $u = u^*/U_{ref}$
U_{ref}	reference velocity, $U_{ref} = (-dP^*/dx^*)H^2/8\mu$ [m/s]
u_s	slip velocity at the wall, $u_s = u_s^*/U_{ref}$
x,y	Cartesian coordinates, $x = x^*/H, y = y^*/H$
z	valance number of ions for a symmetric electrolyte, $z = \lvert z^+\rvert = \lvert z^-\rvert = 1$

Greek symbols

β	slip coefficient, $\beta = \beta^*/H$
δ	electric potential gradient at mid-plane, $\delta = (d\psi/dy)_{y=1/2}$
ε_0	permittivity of vacuum, $\varepsilon_0 = 8.854 \times 10^{-12}$ [C/Vm]
ε_r	relative dielectric constant of the electrolyte, $\varepsilon_r = 78.5$
ϕ	induced electric potential, $\phi = \phi^*/\psi_{ref}$
κ	Debye–Hückel parameter, $\kappa = ze(2n_0/\varepsilon_r\varepsilon_0 k_b T_{ref})^{1/2}$ [m^{-1}]
μ	dynamic viscosity [Ns/m^2]
ρ	fluid density [kg/m^3]
ρ_e	net electric charge density, $\rho_e = \rho_e^*/\rho_{e,ref}$
$\rho_{e,ref}$	reference charge density, $\rho_{e,ref} = zen_0$ [C/m^3]
σ_e	local electrical conductivity, $\sigma_e = \sigma_e^*/\sigma_{ref}$
σ_{av}	average electrical conductivity at cross-section, $\sigma_{av} = \sigma_{av}^*/\sigma_{ref}$
σ_{ref}	reference conductivity, $\sigma_{ref} = Dz^2e^2n_0/k_bT_{ref}$ [$1/\Omega$m]
ψ	electric potential, $\psi = \psi^*/\psi_{ref}$
Ψ	total electric potential, $\Psi = \Psi^*/\psi_{ref}$
ψ_{ref}	reference electrical potential, $\psi_{ref} = k_bT_{ref}/ze$ [V]
ζ	zeta-potential, $\zeta = \zeta^*/\psi_{ref}$

Superscripts and subscripts

*	dimensional quantity
$'$	derivative d/dy
c	mid-plane value
w	at the wall

Experimental studies, which are well reviewed by Neto et al. [15], have shown the existence of significant liquid slip at the walls when low-energy (hydrophobic) surfaces are involved even at low Reynolds numbers ($Re < 10$) [16–20]. Although slip is expected to occur preferentially over very smooth and poorly wetting surfaces, experiments on a variety of solid/liquid interfaces provide evidence of slip lengths up to micron levels in microchannels [17,18]. Slip over rougher walls is attributed to the presence of nano-bubbles trapped on the surface [15], and it is reported that hydrophobic surfaces enhance bubble formation [21].

Recent molecular dynamics simulations of water/solid interfaces indicate that the charged distribution is well approximated with the Poisson–Boltzmann equation in the presence of hydrodynamic slip [22]. Despite the fact that surface charge is expected to promote wetting and reduce slip, experimental observations indicate the presence of significant slip even over highly charged surfaces [4]. Furthermore, Bouzigues et al. [23] presented experimental evidence for slip-induced amplification effects on the wall zeta-potential. It was demonstrated that slip leads to amplification of the zeta-potential by a factor of $(1 + \beta K)$, which indicates considerable increase in zeta-potential especially for larger K. This fact is also confirmed by the theoretical model presented by Chakraborty [24] based on the free energy for binary mixtures.

Slip effects have been studied in microchannel flows, and the results indicate an increase in the mass flow rate and considerable reduction in the applied voltage for electro-osmotic flows [25]. Recently, Park and Choi [26] and Park and Kim [27] studied electro-osmotic flows through hydrophobic microchannels employing an experimentally determined slip velocity at the walls and developed a method for the simultaneous evaluation of the zeta-potential and the slip coefficient.

Electrokinetic flows have been mostly studied in the context of electro-osmotic flows, which involve applied electric fields but no externally applied pressure gradients. In electro-osmotic flows, the induced electric potential due to fluid motion is negligible in comparison to the applied electric potential. On the other hand, in purely pressure-driven flows, a significant electric potential can be generated due to the motion of charged fluid particles, which is called the streaming potential. This potential serves as the basis for possible micro-scale power generators or batteries. The efficiency of such systems is generally low and depends on the fluid properties and the channel geometry [2,28–30]. Larger efficiencies can be achieved when the overlapped EDL regime is considered. However, as mentioned earlier, the P–B equation is not consistent with the true physics of such problems, despite the fact that it has been used by several researches [1–3].

Rather limited information is available in the literature regarding the zeta-potential ζ effects on the streaming potential in purely pressure-driven flows [31–33]. Mirbozorgi et al. [31] performed analytical and numerical studies on the induced potential in planar microchannels. Their results show that, in fully-developed flow, the induced potential increases linearly along the microchannel at a fixed zeta-potential. However, the induced voltage varies in a non-linear manner with ζ such that a maximum voltage is developed with a certain zeta-potential. They have also used the Debye–Hückel approximation in their analytical treatment, which limits the validity of their results to relatively small zeta-potentials. Similar behavior has been reported for flows with variable properties by the numerical study of Hwang and Soong [32]; however, the effect of slip on the induced voltage was not considered in above mentioned studies.

Slip effects on the streaming potential have been studied in the context of electrokinetic energy conversion efficiency in nanochannels with highly overlapped EDLs. Davidson and Xuan [2] numerically studied the electrokinetic conversion efficiency with slip in nanochannels using the Jacobian elliptic function for the potential field. A similar study has been performed by Ren and Stein

[4], where strong enhancement in the energy conversion efficiency has been found in the presence of slip. It must be emphasized that these studies have been carried out for cases where an external load is applied and the net ionic current is not zero, in contrast to seeking the maximum induced voltage with zero net ionic current.

In the present work, the effects of liquid slip at the walls on the streaming potential are studied. Analytical expressions are developed for the velocity field and the induced voltage without invoking the Debye–Hückel approximation. The model used here is based on the non-linear P–B solution for an electrolyte over a single flat plate, which is extended to a planar microchannel. This approach has been previously employed for channel flows, while the precise validity conditions have not been thoroughly examined in the literature. In addition, the commonly ignored variation of electrical conductivity with zeta-potential is examined, and whenever appropriate, the consequences of using the D–H approximation are assessed since it is widely used in the literature.

2. The Poisson–Boltzmann equation

Consider the pressure-driven laminar flow of an electrolyte solution between parallel plates (planar microchannel) as shown in Fig. 1. Electrically neutral liquids may have a distribution of electrical charges near the microchannel walls, known as the electric double layer (EDL). The EDL is primarily a surface phenomenon, which tends to affect the flow field when the typical dimension of the channel is comparable to the EDL thickness. According to the theory of electrostatics, the relationship between the total electric potential Ψ and the local net charge density per unit volume ρ_e at any point in an electrolyte solution is described by the Poisson equation:

$$\nabla^2\Psi = -K^2\rho_e/2 \tag{1}$$

In general, the total electrical potential can be expressed as:

$$\Psi = \psi + \phi \tag{2}$$

where ψ is due to the EDL at an equilibrium state (i.e., no liquid motion and no externally applied electric field) and ϕ is the flow-induced electric potential. It can be shown that for fully-developed conditions, the electrical potential variation in the flow direction can be at most linear [31]. Therefore, $\phi = -E_x x$ where $E_x = -\partial\Psi/\partial x$ is the strength of the electric field. Based on the Boltzmann distribution of charges in the EDL, and in the absence of non-electrical work, the net charge density is given by:

$$\rho_e = -2\sinh(\psi) \tag{3}$$

Substitution of Eq. (3) into the Poisson equation leads to the well-known Poisson–Boltzmann equation:

$$\frac{d^2\psi}{dy^2} = K^2\sinh(\psi) \tag{4}$$

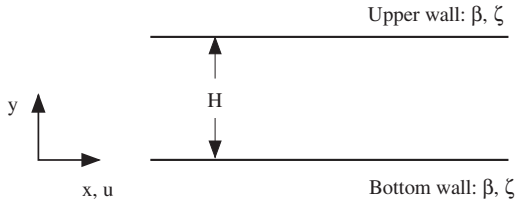

Fig. 1. Planar microchannel geometry and the coordinate system.

where $K = \kappa H = zeH(2n_0/\varepsilon_r\varepsilon_0 k_b T_{ref})^{1/2}$ is the dimensionless Debye–Hückel parameter which is independent of the wall properties and is determined by the electrolyte and the geometric scale of the problem. The electric potential distribution is obtained by solving Eq. (4) subject to appropriate boundary conditions. Subsequently, the charge density distribution ρ_e is determined from Eq. (3).

3. The electric potential field

An explicit analytical expression for the electric potential field is highly desirable in any electrokinetic flow problem. Yet, due to the non-linear nature of the Poisson–Boltzmann equation, a simple closed form solution even in simple microchannels has not been developed. A very common simplification involves the Debye–Hückel approximation $\sinh(\psi)\approx\psi$, which is obviously reasonable only for small ψ. Hunter [6] developed a closed form solution for flow between parallel plates using an overlapping strategy based on the solution of the P–B equation for a single flat plate. However, this solution requires the numerical evaluation of some integrals, which prevent a simple closed form solution that can be directly used in the calculation of the velocity and electric fields. As a remedy, it will be shown here that the solution of the non-linear P–B equation for a flat plate can be adjusted for planar microchannel flows through some modifications to the boundary conditions.

For completeness, some common solutions that are applicable to flat microchannels are given in Table 1 along with the applied boundary conditions and their validity requirements. The Debye–Hückel approximation has been employed in the first and second solutions, which limits their applicability to small zeta-potentials. The second solution is further limited to very thin EDLs or large values of the dimensionless Debye–Hückel parameter, ensuring that the channel mid-plane potential is essentially zero. The third solution is an adaptation of the idea proposed by Philip and Wooding [34] for large zeta-potentials, which was originally developed for the calculation of the potential distribution in cylindrical geometry. Some comments about the accuracy of this solution will be made later. The fourth one, which has been reported by Hunter [6], is an explicit solution to the non-linear P–B equation for a single flat plate subjected to the condition that the potential distribution asymptotically goes to zero far away from the plate. There is no limitation on the value of the zeta-potential. This solution can also be expressed in the following form, which is more useful for the present study:

$$\tanh(\psi/4) = \tanh(\zeta/4)\exp(-Ky) \tag{5}$$

Table 1
Solutions of the Poisson–Boltzmann equation $\psi''(y) = \kappa^2 f(\psi)$.

Case	$f(\psi)$	B.C.	Potential distribution $\psi(y)$	Limitations
1) D–H Approx.	ψ	$\psi(0)=\zeta$, $\psi'(\frac{1}{2})=0$	$\frac{\zeta\cosh(Ky-\frac{K}{2})}{\cosh(\frac{K}{2})}$	$\lvert\zeta\rvert \ll 1$
2) D–H Approx.	ψ	$\psi(0)=\zeta$, $\psi(\frac{1}{2})=0$	$\frac{\zeta\sinh(-Ky+\frac{K}{2})}{\sinh(\frac{K}{2})}$	$\lvert\zeta\rvert \ll 1$, $K\gg 1$
3) Large ζ Approx.	$-\frac{e^{-\psi}}{2}$	$\psi(0)=\zeta$, $\psi'(\frac{1}{2})=\delta$	$2\ln\left[\exp(\frac{\zeta}{2})+\frac{Ky}{2}\right]$	$\lvert\zeta\rvert\gg 0$, $K\gg 1$
4) No D–H Approx.	$\sinh(\psi)$	$\psi(0)=\zeta$, $\psi'(\frac{1}{2})=\delta$	$2\ln\left[\frac{1+\tanh(\frac{\zeta}{4})\exp(-Ky))}{1-\tanh(\frac{\zeta}{4})\exp(-Ky)}\right]$	Contour maps in Fig. 2

$\delta = -2K\sinh(\frac{\psi}{2})$

For a planar microchannel with coordinates as shown in Fig. 1, it is obviously required that $d\psi/dy = 0$ at mid-plane ($y = 1/2$) due to symmetry. This condition is clearly not satisfied by this solution, and therefore, some elaborations on the boundary conditions are required to make it approximately suitable for the present problem. In general, the channel mid-plane electric potential ψ_c is not zero except for very thin EDLs. Therefore, modified boundary conditions are considered here as:

$$y = 1/2 : \psi = \psi_c \text{ and } d\psi/dy = \delta \tag{6}$$

There are more boundary conditions than required; however, these can be related using $d\psi/dy = -2K \sinh(\psi/2)$ obtained from Eq. (5). Hence, it follows that:

$$\delta = -2K \sinh(\psi_c/2) \tag{7}$$

Furthermore, a constraint on the physical parameters can be obtained by applying Eq. (5) at the mid-plane; that is:

$$\tanh(\psi_c/4) = \tanh(\zeta/4)\exp(-K/2) \tag{8}$$

Equation (8) along with the Eq. (7) provides the required criteria for the ranges of K and ζ where Eq. (5) can be applied with reasonable accuracy to a channel flow. Equation (8) has been plotted for three different values of ψ_c in Fig. 2. From this figure, bounds for the zeta-potential and the dimensionless Debye–Hückel parameter can be determined when the mid-plane ψ is specified. The region above each line indicates the applicable values of the D–H parameter and zeta-potential for which the mid-plane potential is less than the specified ψ_c curve. For example, with a zeta-potential of 100 mV, the dimensionless Debye–Hückel parameter must be larger than 22 for the electric potential at the mid-plane to be smaller than 0.001 mV. It is seen that the constraint is almost independent of ζ for large wall potentials.

As mentioned earlier, Dutta and Beskok [10] employed Eq. (5) for the potential distribution in a flat microchannel. However, the range of zeta-potential where this solution is applicable was restricted to $|\zeta^*| < 25$ mV. Fig. 2 indicates that the solution is applicable for this geometry when $|\zeta^*| < 25$ mV if K is large enough. Min et al. [9] proposed a similar contour map but there are some uncertainties about their results since they have obtained a non-zero mid-plane potential for $\zeta = 0$.

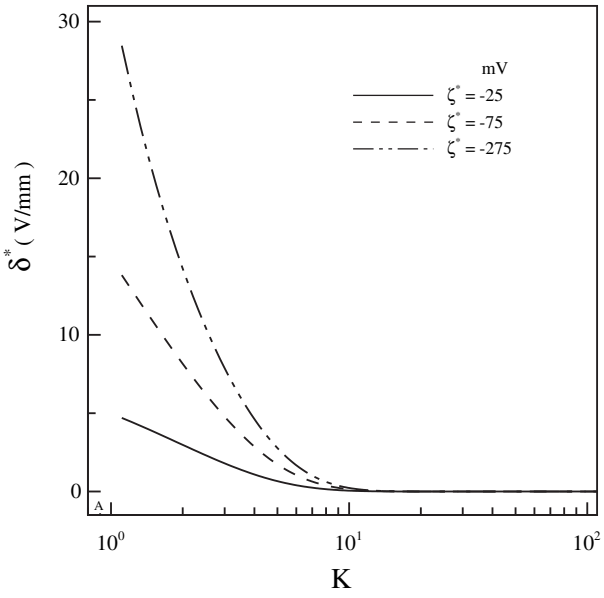

Fig. 3. Mid-plane electric potential gradient δ^* as a function of K for different values of the zeta-potential.

For this approximate solution, it is important to see how well $d\psi/dy = 0$ is satisfied at mid-plane. In Fig. 3, $\delta = d\psi/dy$ is plotted as a function of K for different values of ζ^*. It is observed that for $K > 10$, δ is essentially zero for all zeta-potentials, and thus, the mid-plane boundary condition is well-satisfied. In addition to the boundary condition, the solution accuracy throughout the domain has been examined. In Fig. 4, the normalized electric potential distribution is plotted for $K = 10$ and 20 for $\zeta^* = -75$ mV. It is seen that the solution expressed by Eq. (5) coincides with a full numerical solution of the Poisson–Boltzmann equation (obtained with a 4th order Runge–Kutta method), except in the core region for $K = 10$. It is also notable that the Debye–Hückel approximation

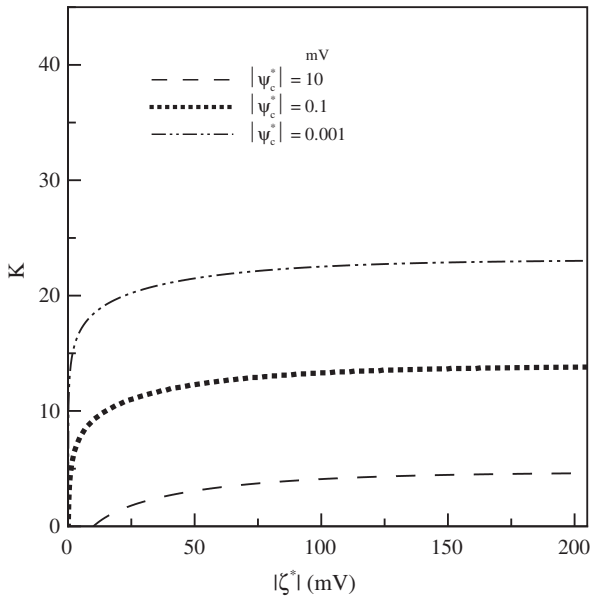

Fig. 2. Contour map associated with Eq. (8).

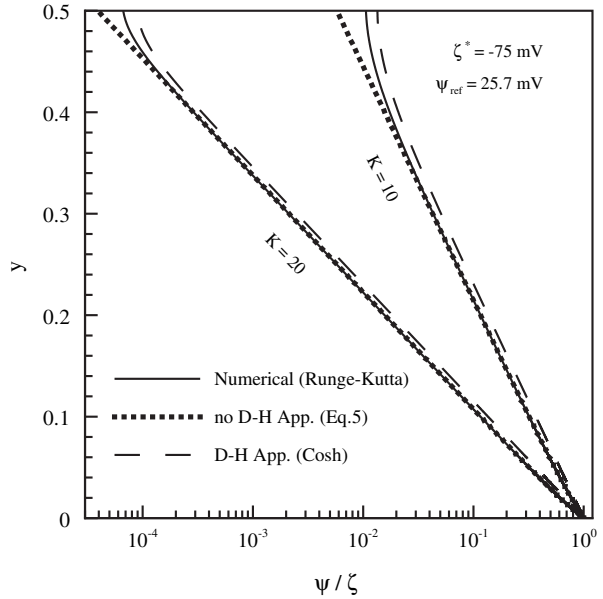

Fig. 4. Comparison of different analytical solutions with the full numerical solution.

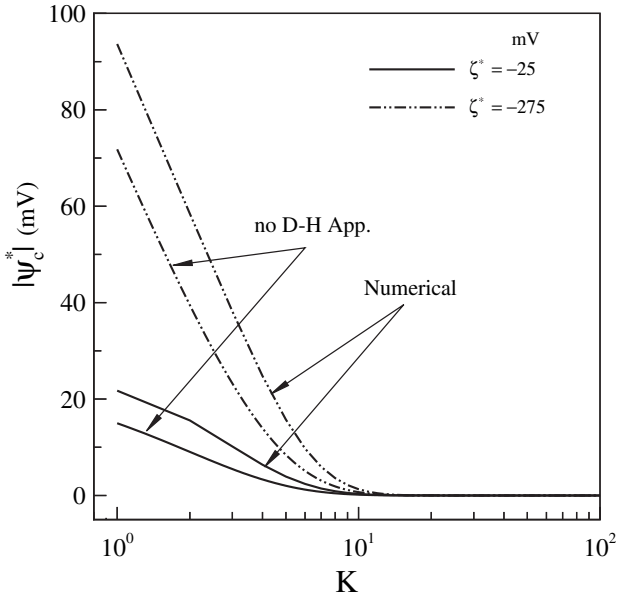

Fig. 5. Comparison of analytical and numerical solutions for the mid-plane electric potential.

leads to a clear deviation from the numerical solution throughout the solution domain, while it satisfies the mid-plane boundary condition of $d\psi/dy = 0$. As indicated by Fig. 3, the analytical solution (Eq. (5)) satisfies the mid-plane boundary condition at larger values of K more accurately, which is also reflected in Fig. 4. This is also confirmed by Fig. 5 where the mid-plane values of the electric potential ψ_c have been plotted for a wide range of the D–H parameter. The calculated values of ψ_c approach the numerical predictions when $K > 10$, essentially independent of ζ.

In order to compare different solutions of the P–B equation listed in Table 1 at large zeta-potentials, a value of $\zeta^* = -150$ mV has been considered. The potential distributions across the channel for $K = 20$ are presented in Fig. 6. The solution offered by Oyanader et al. [35] has been developed numerically following their proposed iterative numerical procedure. Despite the fact that their solution is claimed to be valid at high zeta-potentials, this figure shows that it agrees well with accurate numerical solution only in the region close to the wall, while in the core, it approaches the solution based on the D–H approximation, which is known to perform poorly at high zeta-potentials. However, their solution performs reasonably well at zeta-potentials less than about 75 mV. Note that the analytical solution given by Eq. (5) shows excellent agreement with the full numerical solution of the non-linear P–B equation at high zeta-potentials as well.

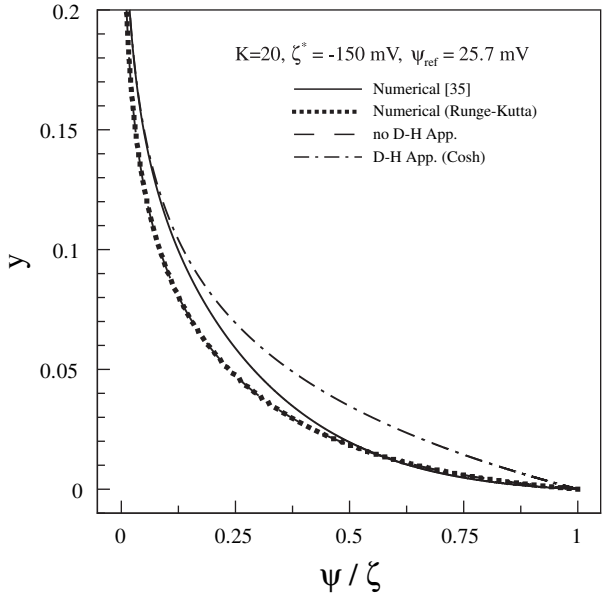

Fig. 6. Comparison of different solutions given in Table 1 with the numerical predictions.

4. The flow field

The solution to the non-linear P–B equation discussed above has been employed for the analytical treatment of slip effects in pressure-driven flows. As will be shown later, the performance of the Debye–Hückel approximation for the prediction of the induced electric field and the associated velocity profile deteriorates further in the presence of slip. For the case of a steady fully-developed liquid flow through a planar microchannel, the equation of motion reduces to:

$$\mu\frac{d^2u^*}{dy^{*2}} - \frac{dP^*}{dx^*} + B\rho_e E_x^* = 0 \tag{9}$$

Using the classical Poiseuille-flow maximum velocity $U_{ref} = (-dP^*/dx^*)(H^2/8\mu)$ as reference, and introducing the charge density from Eq. (1), the momentum equation takes the form:

$$\frac{d^2u}{dy^2} = \frac{2B\mathrm{Re}E_x}{K^2}\left(\frac{d^2\psi}{dy^2}\right) - 8 \tag{10}$$

where $B = k_bT_{ref}n_0/\rho U_{ref}^2$ is the ratio of osmotic pressure to dynamic pressure. Noting that E_x is constant under fully-developed conditions, and solving Eq. (10) with slip at the walls ($u = \beta du/dy$) and symmetry at mid-plane ($du/dy = 0$), the following velocity profile is obtained:

$$u = 4y(1-y) - 4G\left(1 - \frac{\psi}{\zeta}\right) + 4\beta\left(1 - \frac{GK^2q_s}{2\zeta}\right) \tag{11}$$

where $G = B\mathrm{Re}E_x\zeta/2K^2$ and $q_s = \int_0^{1/2}\rho_e(y)dy = -2\psi'(0)/K^2$ is the charge density at the wall. The first term in Eq. (11) is due to the applied pressure gradient. The second term represents the contribution of the EDL to the velocity profile and the third term reflects the slip effect. However, the coefficient G is indirectly related to the slip effect through the resulting induced voltage. From Eq. (11), the slip velocity at the wall is found to be:

$$u_S = 4\beta\left(1 - \frac{GK^2q_S}{2\zeta}\right) = 4\beta\left(1 - \frac{B\mathrm{Re}E_xq_S}{4}\right) \tag{12}$$

For all cases considered here, the following parametric values have been used unless otherwise stated: $Re = 1$, $K = 40$, $\varepsilon_r = 78.5$, $\rho = 10^3$ kg/m^3, $\mu = 10^{-3}$ Ns/m^2, $D = 2\times10^{-9}$ m^2/s, $e = 1.602\times10^{-19}$ C, $n_0 = 6.022\times10^{21}$ ions/m^3, $T = T_{ref} = 298$ K and $z = 1$. Using these, the relevant parameters can be calculated according to $Sc = \mu/\rho D$, $\psi_{ref} = k_bT_{ref}/ze$, $\kappa = ze(2n_0/\varepsilon_r\varepsilon_0k_bT_{ref})^{1/2}$, $H^* = K/\kappa$, $L^* = 10H^*$, $U_{ref} = \mu\mathrm{Re}/\rho H^*$, $B = k_bT_{ref}n_0/\rho U_{ref}^2$, $\Delta P = 8L/\mathrm{Re}$ and $P^* = P\rho U_{ref}^2$ resulting in $Sc = 500$, $\psi_{ref} = 25.7$ mV, $\kappa = 1.04\times10^7$ m^{-1}, $H^* = 3.85$ μm, $L^* = 38.48$ μm, $U_{ref} = 0.26$ m/s, $B = 0.37$, $\Delta P = 80$ and $\Delta P^* = 5.40$ kPa.

In Fig. 7, slip velocities have been plotted as a function of the zeta-potential for three different slip coefficients β. The slip velocities have their maximum values at $\zeta = 0$ and approach zero

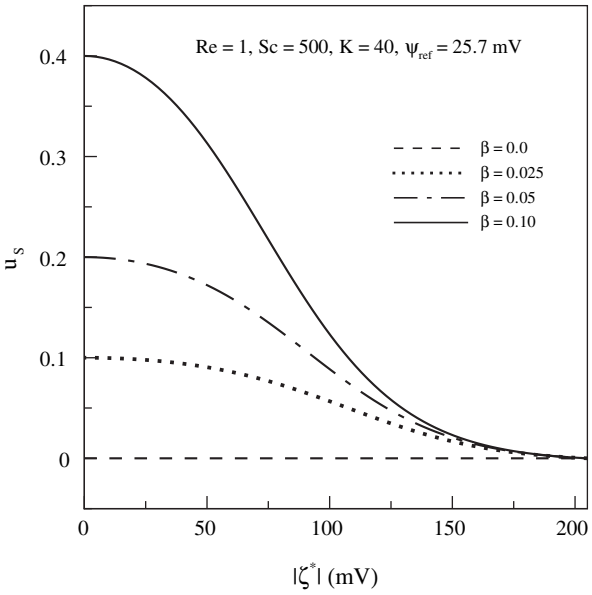

Fig. 7. Slip velocity as a function of zeta-potential for different slip coefficients.

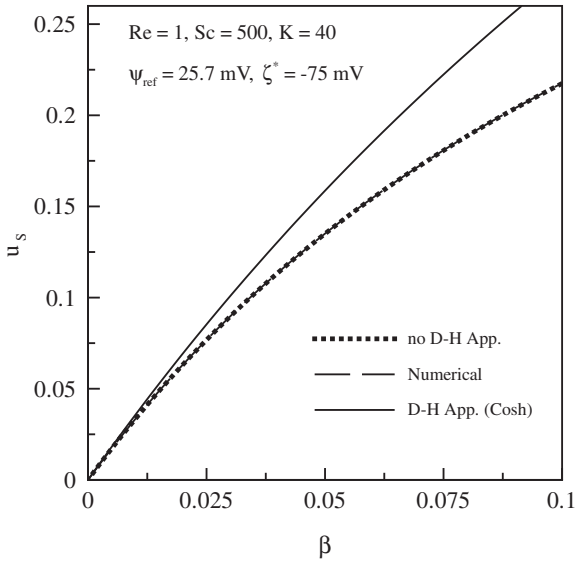

Fig. 9. Slip velocity predictions based on different Poisson–Boltzmann solutions.

with increasing zeta-potential for all β. A similar behavior can be observed in Fig. 8, where the velocity profiles are plotted for various zeta-potentials and a slip coefficient of $\beta = 0.05$ while the other flow parameters remain the same as in Fig. 7. Mathematically, slip reduction with increasing zeta-potential can be explained with the help of Eq. (12). In this equation, it can be shown that the second term in the brackets is always positive and approaches 1 at large ζ. Physically, this effect can be attributed to a stronger binding of the counter-ions to the wall at larger values of ζ, which reduces the mobility of these ions and thus opposes the slip effect at the wall. Fig. 7 also indicates that the slip velocity is almost independent of β for zeta-potentials larger than about 150 mV, while for small $|\zeta^*|$, the slip coefficient affects the slip velocity very significantly.

The performance of the Debye–Hückel approximation weakens in the presence of slip as demonstrated in Fig. 9, where the slip velocity is plotted as a function of β for $\zeta^* = -75$ mV. The solution based on the D–H approximation over-predicts the slip velocity for all β, while the solution given by Eq. (5) shows excellent agreement with the full numerical solution of the non-linear P–B equation.

In Fig. 10, velocity profiles with and without the EDL and slip effects are shown for $\zeta^* = -75$ mV. A comparison between these profiles indicates that the induced voltage opposes the pressure effects, which is more striking in the presence of slip. Therefore, slip can play a more significant role at lower K and higher ζ where stronger EDL effects are present in the flow domain.

5. The induced electric potential

Fluid flow due to an applied pressure gradient in a microchannel results in a down-stream flow of counter-ions concentrated near the channel walls. This causes an electric current (streaming current) in

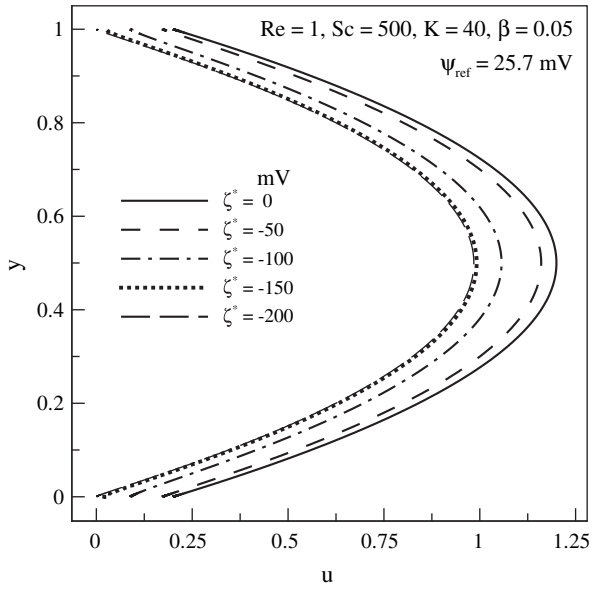

Fig. 8. Effects of zeta-potential on the velocity profile.

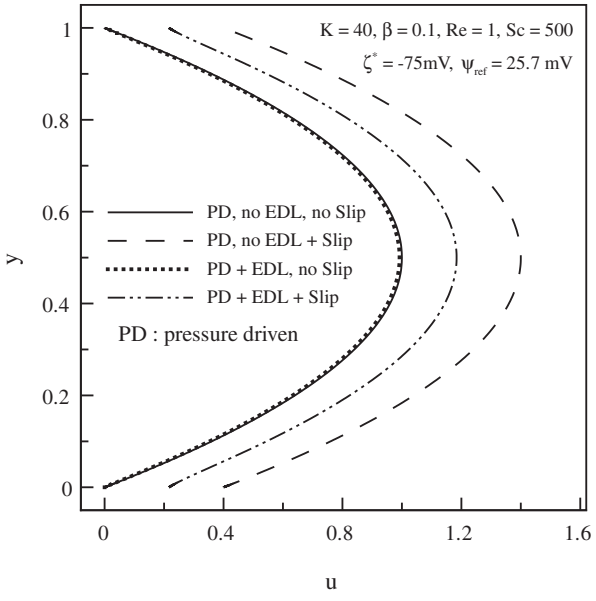

Fig. 10. Slip and EDL effects on the velocity profile.

Table 2
Average conductivity, surface charge density and induced voltage expressions corresponding to the potential distributions given in Table 1.

Case	Average conductivity (σ_{av})	Surface charge density (q_s)	Induced voltage (E_x)
1	2	$2\zeta\frac{\tanh(\omega)}{\omega}$	$\frac{8}{BRe\zeta}\left[\frac{1-\frac{\tanh(\omega)}{\omega}+2\beta\omega\tanh(\omega)}{N\omega^2-1+\frac{\tanh(\omega)}{\omega}+(1+4\beta)\tanh^2(\omega)}\right]$
2	2	$2\zeta\frac{\coth(\omega)}{\omega}$	$\frac{8}{BRe\zeta}\left[\frac{1-\frac{\tanh(\frac{\omega}{2})}{\omega}+2\beta\omega\coth(\omega)}{N\omega^2-1+\frac{\coth(\omega)}{\omega}+(1+4\beta)\coth^2(\omega)}\right]$
3	$\frac{2}{\omega}(e^{-\frac{\zeta}{2}}-1)$	$-\frac{2}{\omega}e^{-\frac{\zeta}{2}}$	$\frac{8}{BRe}\left[\frac{\zeta+\frac{4}{\omega}-2\beta\omega\exp(-\frac{\zeta}{2})}{(\frac{4\omega}{ScB\,Re^2}+\frac{4}{\omega})(-1+\exp(-\frac{\zeta}{2}))+4\beta\exp(-\zeta)}\right]$
4	$2+\frac{8}{\omega}\sinh^2\left(\frac{\zeta}{4}\right)$	$\frac{4}{\omega}\sinh\left(\frac{\zeta}{2}\right)$	$\frac{8}{BRe}\left[\frac{\zeta-(\frac{4}{\omega})S(\zeta)+4\beta\omega\sinh(\frac{\zeta}{2})}{N(\omega\zeta)^2+(\frac{32}{\omega})\sinh^2(\frac{\zeta}{4})+16\beta\sinh^2(\frac{\zeta}{2})}\right]$

$\omega=\frac{K}{2}$; $N=\frac{2\sigma_{av}}{BScRe^2\zeta^2}$; $S(\zeta)=\sum_{i=1}^{\infty}\frac{(\tanh(\frac{\zeta}{4}))^{2i}}{4i^2}=\frac{1}{4}\tanh^2\left(\frac{\zeta}{4}\right)+\frac{1}{16}\tanh^4\left(\frac{\zeta}{4}\right)+\frac{1}{36}\tanh^6\left(\frac{\zeta}{4}\right)+\cdots$

the flow direction with a density of $J_s(y)=\rho_e(y)u(y)$ per unit area. The streaming potential, or the induced voltage associated with this streaming current, establishes a current in the opposite direction called the conduction current with a density of $J_c(y)=(E_x/ReSc)\sigma_e(y)$ where $\sigma_e(y)=2\cosh(\psi)$ is the electrical conductivity. For steady fully-developed conditions, the cross-sectional average of the electric current in the flow direction must be equal to zero. That is, the streaming current density must be balanced by the conduction current density, which can be expressed in non-dimensional form as follows:

$$2\int_0^{1/2}\rho_e(y)u(y)dy+\frac{E_x\sigma_{av}}{ReSc}=0 \tag{13}$$

where σ_{av} is the average electrical conductivity at any cross-section given by:

$$\sigma_{av}=2\int_0^{1/2}\sigma_e(y)dy=4\int_0^{1/2}\cosh(\psi)dy=2+2\int_0^{1/2}\left(\frac{\psi'}{K}\right)^2dy \tag{14}$$

The last equality in Eq. (14) follows from the first integration of Eq. (4). It can be also shown that $\cosh(\psi)=1-(\psi'/K)\sinh(\psi/2)$, which leads to:

$$\sigma_{av}=2+\frac{16}{K}\sinh^2(\zeta/4) \tag{15}$$

It should be noted that the second term in the Eq. (15) is frequently neglected in literature and the dependency of σ_{av} on ζ is generally ignored. Substituting $u(y)$ into Eq. (13) and employing the mathematical properties of the P–B equation similar to those used in Eq. (14), the induced voltage E_x can be expressed as:

$$E_x=\frac{8K^2}{BRe}\left(\frac{\zeta-2\int_0^{1/2}\psi dy+\beta K^2q_S/2+\delta(1+4\beta)/4}{\frac{\sigma_{av}K^4}{2BScRe^2}+4\int_0^{1/2}(\psi')^2dy+\beta K^4q_S^2+4\delta\left(\psi_c-\delta+\beta K^2q_S\right)}\right) \tag{16}$$

For $K<10$, according to Figs. (3) and (5), both ψ_c and δ approach zero. Thus, Eq. (16) becomes:

$$E_x=\frac{8K^2}{BRe}\left(\frac{\zeta-2\int_0^{1/2}\psi dy+\beta K^2q_S/2}{\frac{\sigma_{av}K^4}{2BScRe^2}+4\int_0^{1/2}(\psi')^2dy+\beta K^4q_S^2}\right) \tag{17}$$

The final expression for the induced voltage is obtained upon substitution of the potential distribution ψ from Table 1 into Eq. (17) and performing the integration. This final form is given in Table 2 along with other important parameters employed in Eq. (17).

In the literature, it is commonly assumed that $\sigma_{av}=2$ for small values of ζ based on the first order approximation $\cosh(\psi)\approx1$ in Eq. (14). Fig. 11 indicates that this assumption is valid for zeta-potentials up to about 50 mV. It should be noted that a closed form expression for σ_{av} cannot be obtained when the Debye–Hückel approximation is employed (case 1), while the analytical treatment of the problem without this approximation leads to the closed form expressions given in Table 2. Mirbozorgi et al. [31] have also examined case 1 subject to the no-slip condition $\beta=0$ and reported that $\sigma_{av}=2$ is problematic in the calculation of E_x. It was found that more accurate results can be obtained by evaluating σ_{av} through a numerical integration of Eq. (14) using the potential distribution associated with this case. A similar procedure has been adopted in the present study for evaluating σ_{av} for case 1. As shown in Fig. 11, σ_{av} based on the present solution (case 4) agrees well with the numerical result even at large zeta-potentials. For zeta-potentials higher than about 100 mV, electrical conductivity varies exponentially with the zeta-potential. Fig. 11 also shows that the D–H approximation leads to a very significant over prediction of electrical conductivity at higher ζ.

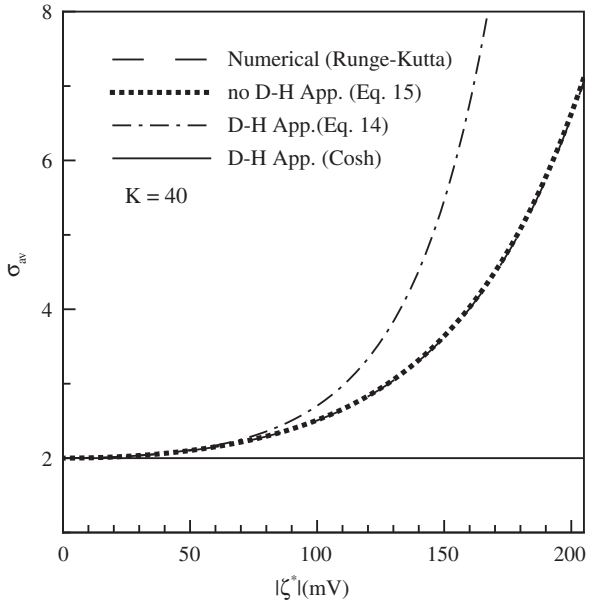

Fig. 11. Average electrical conductivity as a function of zeta-potential.

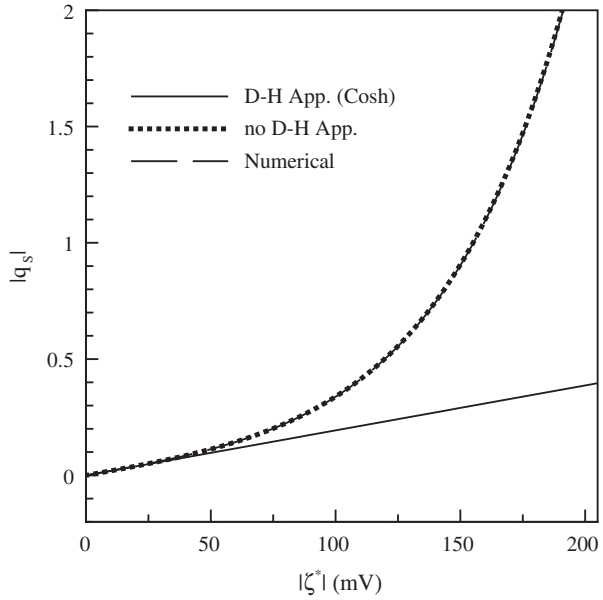

Fig. 12. Surface charge density as a function of zeta-potential.

Fig. 12 shows the surface charge density q_S as a function of the zeta-potential with and without the Debye–Hückel approximation. The surface charge density is introduced to the problem through the slip boundary condition when expressed in the form of a velocity gradient, $u_s = \beta du/dy|_w$. Therefore, in the absence of slip or when u_s is specified directly, q_s does not appear in the velocity profile, and consequently, in the induced voltage, Eq. (17). Fig. 12 shows that the D–H approximation leads to an accurate prediction of q_s only for zeta-potentials lower than about 50 mV.

In Fig. 13, the variations of induced voltage for two different values of K have been compared to the solutions given in Table 2 when velocity slip is absent. Despite the differences in the mathematical expressions for cases 1 and 2, their numerical values are essentially identical for $K > 10$. This figure shows that a larger potential is induced with lower values of K (thicker EDL), and more importantly, E_x decreases rapidly with increasing zeta-potential after reaching a maximum value. This reduction is due to the exponential increase in electrical conductivity at higher zeta-potentials (see Fig. 11) that opposes the induced voltage by increasing the conduction current. At high zeta-potentials, strong conduction currents basically cause the induced voltage to vanish. It is also observed that as K decreases, maximum E_x occurs at lower ζ.

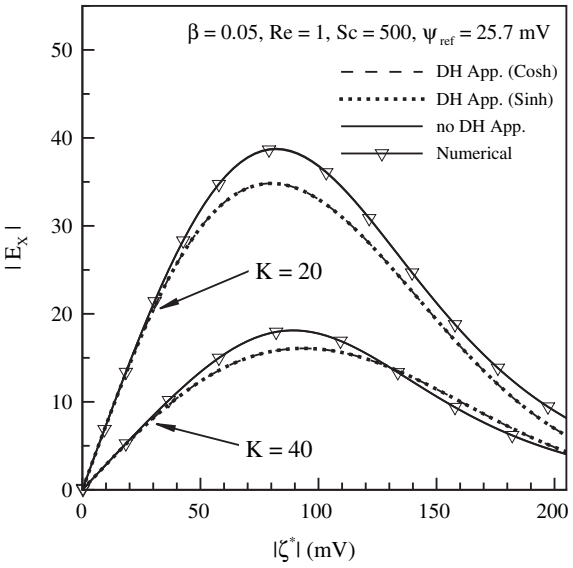

Fig. 14. Induced voltage variations in the presence of slip.

Slip is expected to increase the induced voltage by enhancing advection near the wall. In Fig. 14, the induced voltage variations as a function of zeta-potential are plotted for the same conditions as those in Fig. 13 for a slip coefficient of $\beta = 0.05$. Almost an 100% increase in the maximum induced voltage is observed at this slip coefficient. Both figures indicate that the Debye–Hückel approximation deviates from the numerical solution at zeta-potentials higher than 50 mV. The deviation occurs at even lower values of ζ

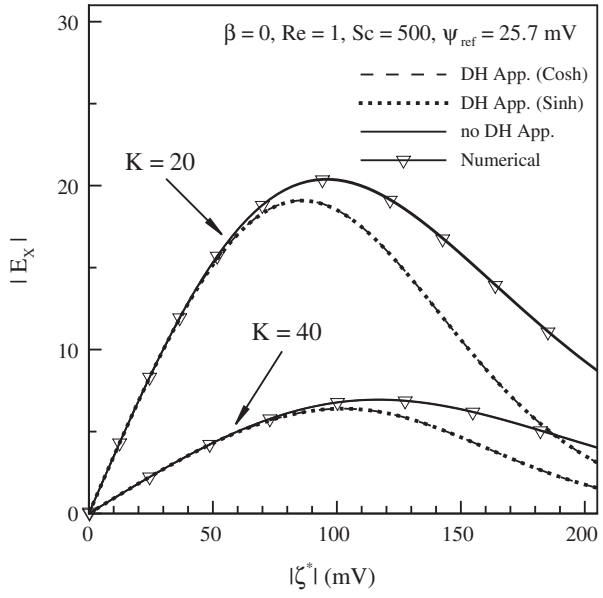

Fig. 13. Induced voltage variations under the no-slip assumption.

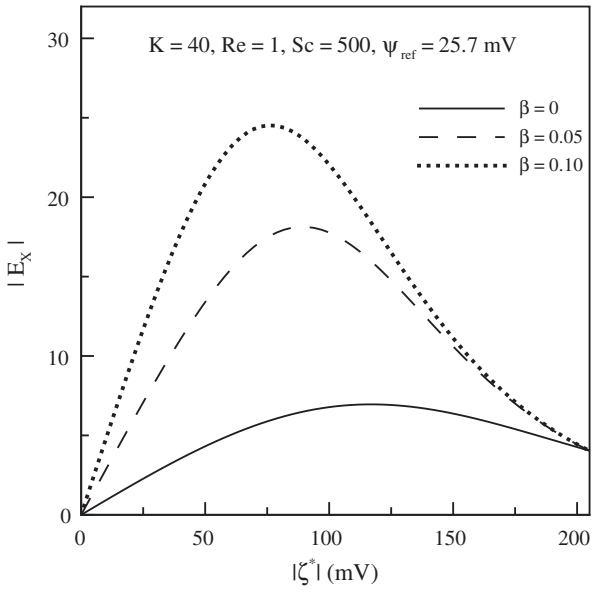

Fig. 15. Induced voltage as a function of zeta-potential for various slip coefficients.

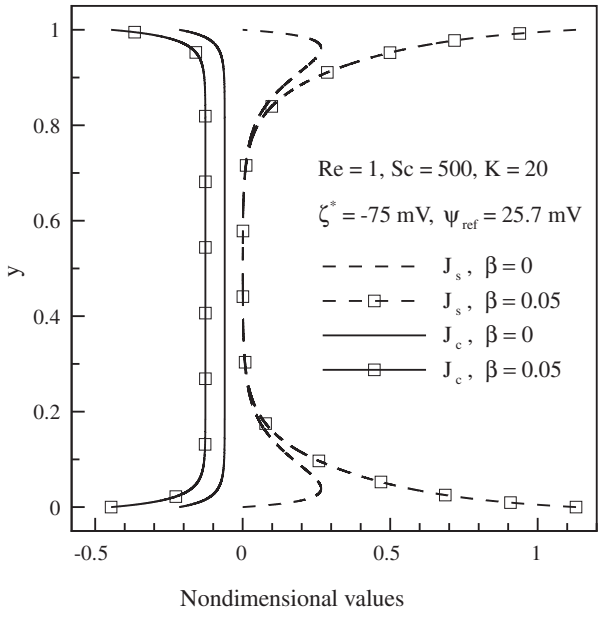

Fig. 16. Slip effects on the streaming and conduction currents.

when slip is present. It is seen that the induced voltage is underestimated with the Debye–Hückel approximation even in the range of its validity.

To further clarify the effects of slip on the induced voltage, three different slip coefficients have been considered in Fig. 15. The flow parameters are the same as those in Fig. 14. As expected, slip dramatically increases the induced voltage, which is also accompanied by shifting the point of maximum voltage to lower zeta-potentials. For example, at $\zeta^* = -100$ mV, this figure shows that the non-dimensional induced voltages are 6.8 and 22 for cases without and with slip ($\beta = 0.1$), respectively. For the microchannel data given in section 4, these values correspond to 45.3 mV/mm and 147.2 mV/mm; and for an applied pressure difference of $\Delta P^* = 54$ kPa, the induced voltages are found to be 1.74 V and 5.67 V, respectively, over the length of microchannel. From Figs. 14 and 15 it is clear that the values of the maximum voltage and their locations are strongly dependent on the slip coefficient as well as K. Increasing K reduces the maximum induced voltage and shifts its location slightly to higher zeta-potentials, which is in contrast to the slip effects.

Finally, the cross-sectional distribution of the electric current density and its components are compared for cases with and without slip in Fig. 16. The streaming current density J_s depends on the net charge density and the flow velocity according to $J_s(y) = \rho_e(y)u(y)$. For the no-slip condition, zero-velocity at the wall leads to $J_{s,w} = 0$ despite the maximum charge density there. For large K, the streaming current density vanishes rapidly away from the wall as the net charge density vanishes. Therefore, for the no-slip condition, the maximum streaming current density is encountered close to the wall as seen in this figure. In the presence of slip, the fluid at the wall is in motion, and hence, the maximum streaming current density occurs in the immediate vicinity of the wall. This leads to a major increase in the cross-sectional average of the streaming current density as described earlier.

6. Conclusions

In this study, the conditions under which the non-linear P–B solution for the electric potential field in an electrolyte solution over a single flat plate can be extended to a planar microchannel have been examined. The validity ranges of the key parameters where this solution can be accurately applied have been identified. Employing this solution, the Navier–Stokes equations were solved for pressure-driven flows in the presence of velocity slip at the walls. Analytical expressions for the velocity profile, induced voltage, average electrical conductivity, and surface charge density are presented without invoking the Debye–Hückel approximation.

It is shown that the induced voltage reaches a maximum value at a specific zeta-potential depending on the slip coefficient and the dimensionless Debye–Hückel parameter, while decreasing at higher zeta-potentials due to a rapid increase in the average electrical conductivity, which is highly underestimated when the widely used Debye–Hückel approximation is invoked. Present study shows clearly that the induced voltage increases very significantly with velocity slip at the walls, which indicates that the efficiency of microfluidic power generators/batteries can be greatly improved through the use of hydrophobic surfaces.

Acknowledgment

M. Renksizbulut gratefully acknowledges the financial support of the Natural Sciences and Engineering Research Council of Canada.

References

[1] S.H. Behrens, M. Borkovec, Exact Poisson–Boltzmann solution for the interaction of dissimilar charge-regulating surfaces. Physical Review E 60 (6) (1999) 7040–7048.
[2] C. Davidson, X. Xuan, Electrokinetic energy conversion in slip nanochannels. Journal of Power Sources 179 (2008) 297–300.
[3] C. Davidson, X. Xuan, Effects of Stern layer conductance on electrokinetic energy conversion in nanofluidic channels. Electrophoresis 29 (2008) 1125–1130.
[4] Y. Ren, D. Stein, Slip-enhanced electrokinetic energy conversion in nanofluidic channels. Nanotechnology 19 (2008) 195707(6).
[5] F.H. Van Der Heyden, D. Stein, K. Besteman, S.G. Lemay, C. Dekker, Charge inversion at high ionic strength studied by streaming currents. Physical Review Letters 96 (22) (2006) 224502(4).
[6] R.J. Hunter, Zeta-potential in Colloid Science: Principles and Applications. Academic Press, London, 1981.
[7] X. Wang, J. Wu, Flow behavior of periodical electroosmosis in microchannel for biochips. Journal of Colloid and Interface Science 293 (2) (2006) 483–488.
[8] P. Dutta, K. Horiuchi, H.M. Yin, Thermal characteristics of mixed electroosmotic and pressure-driven microflows. Computers and Mathematics with Applications 52 (5) (2006) 651–670.
[9] J.Y. Min, D. Kim, S.J. Kim, A novel approach to analysis of electroosmotic pumping through rectangular-shaped microchannels. Sensors and Actuators B: Chemical 120 (1) (2006) 305–312.
[10] P. Dutta, A. Beskok, Analytical solution of combined electroosmotic/pressure driven flows in two-dimensional straight channels: finite Debye layer effects. Analytical Chemistry 73 (9) (2001) 1979–1986.
[11] W. Qu, D. Li, A model for overlapped EDL fields. Journal of Colloid and Interface Science 224 (2000) 397–407.
[12] P. Biesheuvel, Simplifications of the Poisson–Boltzmann equation for the electrostatic interaction of close hydrophilic surfaces in water. Journal of Colloid and Interface Science 238 (2) (2001) 362–370.
[13] F. Baldessari, Electrokinetics in nanochannels. Part I. Electric double layer overlap and channel-to-well equilibrium. Journal of Colloid and Interface Science 325 (2) (2008) 526–538.
[14] S. Talapatra, S. Chakraborty, Double layer overlap in ac electroosmosis. European Journal of Mechanics, B/Fluids 27 (3) (2008) 297–308.
[15] C. Neto, D.R. Evans, E. Bonaccurso, H.J. Butt, V.S. Craig, Boundary slip in Newtonian liquids: a review of experimental studies. Report on Progress in Physics 15 (2005) 2859–2897.
[16] J.-T. Cheng, N. Giordano, Fluid flow through nanometer-scale channels. Physical Review E – Statistical, Nonlinear, and Soft Matter Physics 65 (3) (2002) 031206(5).
[17] D.C. Tretheway, C.D. Meinhart, A generating mechanism for apparent fluid slip in hydrophobic microchannels. Physics of Fluids 16 (5) (2004) 1509–1515.
[18] Y. Zhu, S. Granick, Rate-dependent slip of Newtonian liquid at smooth surfaces. Physical Review Letters 87 (9) (2001) 96105(4).
[19] J.K. Holt, H.G. Park, Y. Wang, M. Stadermann, A.B. Artyukhin, C.P. Grigoropoulos, A. Noy, O. Bakajin, Fast mass transport through sub-2-nanometer carbon nanotubes. Science 312 (5776) (2006) 1034–1037.
[20] M. Majumder, N. Chopra, R. Andrews, B.J. Hinds, Nanoscale hydrodynamics: enhanced flow in carbon nanotubes. Nature 438 (7064) (2005) 44.

[21] J.W. Tyrrel, P. Attard, Images of nanobubbles on hydrophobic surfaces and their interactions. Physical Review Letters 87 (17) (2001) 176104(4).
[22] L. Joly, C. Ybert, E. Trizac, L. Bocquet, Liquid friction on charged surfaces: from hydrodynamic slippage to electrokinetics. Journal of Chemical Physics 125 (20) (2006) 204716(14).
[23] C.I. Bouzigues, P. Tabeling, L. Bocquet, Nanofluidics in the debye layer at hydrophilic and hydrophobic surfaces. Physical Review Letters 101 (11) (2008) 114503(4).
[24] S. Chakraborty, Generalization of interfacial electrohydrodynamics in the presence of hydrophobic interactions in narrow fluidic confinements. Physical Review Letters 100 (9) (2008) 097801(4).
[25] J. Yang, D.Y. Kwok, Effect of liquid slip in electrokinetic parallel-plate microchannel flow. Journal of Colloid and Interface Science 260 (1) (2003) 225–233.
[26] H. Park, Y. Choi, A method for simultaneous estimation of inhomogeneous zeta potential and slip coefficient in microchannels. Analytica Chimica Acta 616 (2) (2008) 160–169.
[27] H. Park, T. Kim, Simultaneous estimation of zeta potential and slip coefficient in hydrophobic microchannels. Analytica Chimica Acta 593 (2) (2007) 171–177.
[28] F.H. Van Der Heyden, D.J. Bonthuis, D. Stein, C. Meyer, C. Dekker, Power generation by pressure-driven transport of ions in nanofluidic channels. Nano Letters 7 (4) (2007) 1022–1025.
[29] W. Olthuis, B. Schippers, J. Eijkel, A. Van Den Berg, Energy from streaming current and potential. Sensors and Actuators B: Chemical 111–112 (Suppl.) (2005) 385–389.
[30] H. Daiguji, P. Yang, A.J. Szeri, A. Majumdar, Electrochemomechanical energy conversion in nanofluidic channels. Nano Letters 4 (12) (2004) 2315–2321.
[31] S.A. Mirbozorgi, H. Niazmand, M. Renksizbulut, Streaming electric potential in pressure-driven flows through reservoir-connected microchannel. Journal of Fluids Engineering, Transactions of the ASME 129 (10) (2007) 1346–1357.
[32] P. Hwang, C. Soong, Investigation of variable-property microchannel flows with electro-thermo-hydrodynamic interactions at constant pressure gradient or constant flow rate. International Journal of Heat and Mass Transfer 51 (1–2) (2008) 210–223.
[33] S. Chakraborty, S. Das, Streaming-field-induced convective transport and its influence on the electroviscous effects in narrow fluidic confinement beyond the Debye–Hückel limit. Physical Review E – Statistical, Nonlinear, and Soft Matter Physics 77 (3) (2008) 037303.
[34] J.R. Philip, R.A. Wooding, Solution of the Poisson–Boltzmann equation about a cylindrical particle. Journal of Chemical Physics 52 (1970) 953–959.
[35] M. Oyanader, P. Arce, A new and simpler approach for the solution of the electrostatic potential differential equation. Enhanced solution for planar, cylindrical and annular geometries. Journal of Colloid and Interface Science 284 (1) (2005) 315–322.